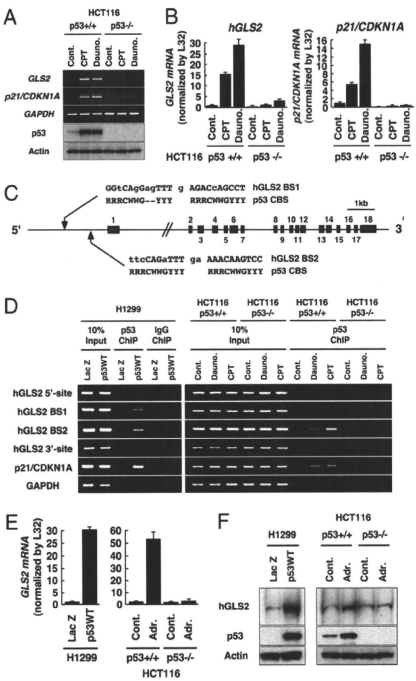

Fig. 1. Identification of phosphate-activated GLS (GLS2) as a p53-inducible gene. (*A*) HCT116 ($p53^{+/+}$) or ($p53^{-/-}$) cells were treated with camptothecin (CPT; 300 nM) or daunorubicin (Dauno; 200 nM). RT-PCR analysis for *GLS2*, *p21/CDKN1A*, and *GAPDH* expression (top three panels) and immunoblotting to detect p53 (DO1) and actin (Sigma; bottom two panels) were performed. (*B*) HCT116 cells were treated with indicated agents as in *A*. Total RNA was subjected to real-time RT-PCR analysis. Expression levels of *GLS2* (*Left*) and *p21/CDKN1A* (*Right*) RNAs were determined by the comparative threshold cycle method and then normalized by *L32* expression. (*C*) Genomic structure of human *GLS2 with* its exon/intron organization and two potential p53 binding sites upstream of the first exon (*GLS2* BS1 and *GLS2* BS2) compared with the canonical p53 binding site. R, purine; Y, pyrimidine; W, adenine or thymine. (*D*) H1299 cells infected with adenoviruses expressing either LacZ or p53 (p53WT) for 24 h (*Left*) and HCT116 ($p53^{+/+}$) or ($p53^{-/-}$) cells either not treated (Control) or treated with daunorubicin (200 nM) or CPT (300 nM) for 24 h (*Right*) were processed for ChIP assays using anti-p53 (DO1/1801) or control IgG (Santa Cruz Biotechnology), followed by the amplification of p53 binding sites as indicated. (*E*) H1299 cells (*Left*) were infected with adenoviruses expressing either LacZ or p53 (p53WT) or HCT116 cells ($p53^{+/+}$; *Right*) or ($p53^{-/-}$) cells were treated with doxorubicin (Adr., 0.3 μM) for 24 h. Expression level of GLS2 mRNA was determined as in *B*. (*F*) Cells were treated as in *E* and subjected to mitochondrial fractionation. Immunoblotting was performed to detect GLS2 protein in the mitochondrial fraction and p53 and actin from whole extracts.

size of GLS2 (Fig. S4) (17). As GLS2 was shown to be a mitochondrial enzyme (18), we isolated mitochondria, and immunoblotting showed that GLS2 protein induced by p53 was in that fraction (Fig. 1*F*). Both ectopically expressed FLAG-tagged GLS2 in H1299 cells and endogenous GLS2 in daunorubicin-treated human aorta endothelial cells (HAECs) displayed a cytoplasmic particulate staining pattern, indicative of mitochondrial localization (Fig. S5 *A* and *B*).

Normal cells (HAEC and TIG-7) as well as tumor cell lines expressing WT p53 (HCT116, MCF-7, and U2OS) were subjected to treatments that cause oxidative genotoxic damage, and GLS2 induction was assessed by real-time PCR analysis (Fig S5 *C–F*). GLS2 was confirmed to be a p53 target gene in both nontumor and tumor cells, although the extent of its up-regulation differed depending on the cell type or the levels and nature of the stress.

p53 and GLS2 Modulate Intracellular ROS Levels and the GSH/GSSG Ratio in Cells. p53 has been reported to have opposing roles in the regulation of ROS through transactivation of antioxidant and prooxidant genes, each of which contribute to the tumor suppressor function of p53 (19, 20). As previously reported (19), basal ROS levels were suppressed (approximately by half) in exponentially cultured HCT116 ($p53^{+/+}$) cells or in cells treated with low concentrations of doxorubicin (0.03–0.3 μM) compared with HCT116 ($p53^{-/-}$) cells (Fig. 2*A*). In contrast, at higher doses of doxorubicin (>1 μM), $p53^{+/+}$ cells showed a relative increase in ROS, indicating that p53 differentially regulates ROS levels depending on the severity of the stress signal. Accordingly, whereas *GLS2* and *p21/CDKN1A* were induced at lower concentrations of doxorubicin, a prooxidant gene such as *PUMA* was induced only at relatively high concentrations of this drug (Fig. 2*B*). Thus, WT p53-expressing cells are more tolerant of low doses of oxidative stress compared with p53-negative cells. During acute stress conditions, however, p53 facilitates increased intracellular ROS levels and apoptosis.

We next examined the effect of p53 or GLS2 silencing on ROS levels with or without cellular stress in both carcinoma and normal cells (Fig. 2 *C–E*). GLS2 siRNA reduced GLS2 levels by approximately 90% without affecting p53 protein levels or p53 target gene induction (Fig. S6). Down-regulation of p53 or GLS2 increased ROS levels significantly in both unstressed and doxorubicin-treated U2OS cells (Fig. 2 *C* and *D*). Similarly, p53 or GLS2 silencing in normal primary HAEC cells led to increased ROS in both untreated and DNA damaged cells (Fig. 2*E*) whereas expression of FLAG-tagged GLS2 led to a significant reduction of both basal ROS levels and ROS levels in DNA-damaged H1299 cells (Fig. 2*F*). Thus, p53 and GLS2 are directly involved in ROS regulation and antioxidant defense. The antioxidant or prooxidant outcomes of p53 activation are likely to depend on the differential regulation of p53 targets, including GLS2.

Glutamine is catabolized by GLS2 to glutamate, one of the precursor amino acids in the biosynthesis of GSH, and GSH/oxidized glutathione (GSSG) is the major redox couple that determines the antioxidative capacity of cells (21). Glutamine preserves total GSH levels after oxidative damage, making it a component of the cellular antioxidant defense (22). GLS2 plays a critical role by up-regulating GSH levels upon oxidative stress (23, 24). Overexpression of 3×FLAG–GLS2 increased glutamine consumption and facilitated the production of glutamate detected in the culture medium of H1299 cells, thus confirming its enzymatic function to catabolize glutamine to glutamate (Fig. 3*A*). Conversely, down-regulation of GLS2 decreased the glutamine consumption rate in H1299 cells expressing Adp53 at low levels in which apoptosis was not induced (Fig. 3*B Left*). Consistently, the induction of p53 led to increased glutamate production, whereas silencing of GLS2 attenuated the glutamate production rate significantly in H1299 cells (Fig. 3*B Right*), supporting the role of GLS2 in p53-dependent intracellular glutamine metabolism.

Further, overexpression of 3×FLAG–GLS2 increased GSH/GSSG ratios in both unstressed and daunorubicin or camptothecin-treated H1299 cells (Fig. 3*C*). In contrast, down-regulation of GLS2 or p53 suppressed the GSH/GSSG ratio in unstressed and doxorubicin-treated U2OS cells (Fig. 3*D*). Last, consistent with previous results, HCT116 ($p53^{+/+}$) cells had a higher GSH/GSSG ratio and more intracellular ROS than HCT116 ($p53^{-/-}$) cells (Fig. 3 *E* and *G*

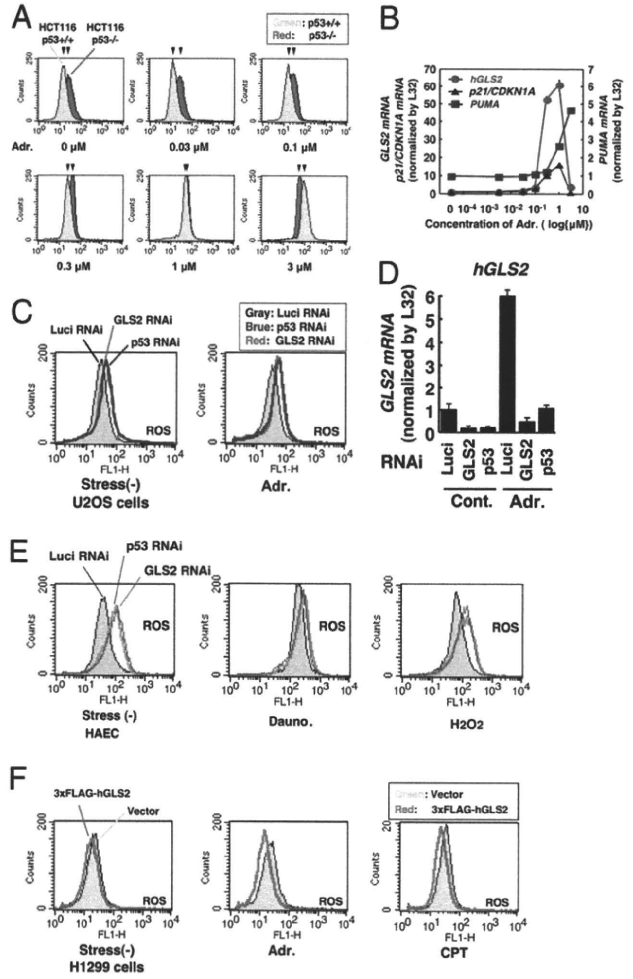

Fig. 2. Modulation of GLS2 or p53 expression affects intracellular ROS levels. (*A*) HCT116 cells that either express p53 ($p53^{+/+}$ in green) or lack p53 ($p53^{-/-}$ in red) were treated with the indicated doses of doxorubicin for 24 h and then subjected to DCF staining followed by FACS analysis. (*B*) HCT116 $p53^{+/+}$ cells were treated with indicated dose of doxorubicin as in *A*. Expression levels of GLS2, p21/CDKN1A, and PUMA mRNAs were determined as in Fig. 1*B*. (*C*) U2OS cells were transfected with luciferase RNAi (Luci RNAi; gray), p53 RNAi (blue), or GLS2 RNAi (red) for 24 h and then cells were either not treated (stress –; *Left*) or treated with doxorubicin (100 nM; *Right*) for 24 h. DCF staining was followed by FACS analysis. (*D*) U2OS cells were transfected with indicated RNAi and then treated with doxorubicin as in *C*. Expression levels of GLS2 mRNA were determined as in Fig. 1*B*. (*E*) HAEC cells were transfected as in *C* and then either not treated (stress –) or treated with daunorubicin (100 nM) or H_2O_2 (0.1 mM) for 24 h. DCF staining was followed by FACS analysis. (*F*) Cells were transfected with indicated DNA for 48 h. After the selection in the presence of 600 μg/mL G418 for 5 d, cells were split, cultured for 24 h, and then not treated (stress –) or treated with doxorubicin or CPT for another 24 h. DCF staining was followed by FACS analysis.

Left). Depletion of glutamine in the medium decreased the GSH/GSSG ratio strongly and up-regulated intracellular ROS levels in HCT116 ($p53^{+/+}$) cells (Fig. 3 *F* and *G Right*). Together, these data indicate that GLS2 regulates glutamine metabolism to control ROS through the GSH-dependent antioxidant system.

GLS2 Protects Cells from DNA Oxidation and ROS-Sensitive Apoptosis. High levels of ROS lead to formation of 8-hydroxy-2′-deoxyguanosine (8-OH-dG), the main source of oxidation-associated mutagenesis (25). Consistent with the intracellular ROS levels seen in HCT116 ($p53^{-/-}$) cells in unstressed conditions (Fig. 3*G Left*), these p53-negative cells displayed approximately twofold higher 8-OH-dG levels compared with HCT116 ($p53^{+/+}$) cells (Fig. 4 *A* and *B*). Following daunorubicin treatment, which significantly up-regulated ROS levels in these cells (Fig S7*A*), 8-OH-dG levels in HCT116 ($p53^{-/-}$) cells increased to a greater extent than in HCT116 ($p53^{+/+}$) cells (Fig. 4 *A* and *B*). Down-regulation of p53 or GLS2 increased 8-OH-dG to levels comparable to those observed in the HCT116 ($p53^{-/-}$) cells in both untreated and daunorubicin-treated cells (Fig. 4*C*) or U2OS cells that contain WT p53 (Fig. 4*D*). Furthermore, overexpression of GLS2 in H1299 cells suppressed 8-OH-dG levels (Fig S7*B*). Thus, p53-mediated induction of GLS2 contributes to the antioxidant function of p53 by lowering intracellular ROS levels and thereby preventing DNA oxidation.

Intracellular ROS levels can affect the sensitivity of cells to p53-dependent apoptosis (26). Although GLS2 down-regulation slightly increased apoptosis in p53-deficent cells, reduced GLS2 expression led to a larger increase in apoptosis in both unstressed and daunorubicin-treated ($p53^{+/+}$) cells (Fig. 4*E*). Accordingly, the antioxidant compound N-acetylcysteine lowered GLS2 siRNA-enhanced apoptosis in U2OS cells (Fig. S8). Based on these data, we propose that GLS2 functions to reduce cellular sensitivity to ROS-associated apoptosis (Fig. 4*F*).

A Potential Tumor-Suppressor Role for GLS2. Overexpression of FLAG-tagged GLS2 in H1299 cells led to a significant reduction of growth (Fig. 5*A*) as well as colony formation ability (Fig. 5*B*). Importantly, expression of GLS2 mRNA was significantly decreased in most of 12 specimens from hepatocellular carcinomas and metastatic liver tumors from colon cancers compared with liver tissues with chronic hepatitis ($n = 6$) or adjacent normal liver tissues ($n = 6$; Fig. 5*C*). Along with the fact that the expression of GLS2 is reduced in many brain tumors such as glioblastoma and anaplastic astrocytomas (27), these data suggest that GLS2 plays a role in tumor suppression.

Discussion

Although GLS2 was originally thought to be present only in adult liver tissue (28), emerging evidence has revealed that *GLS2* expression also occurs in extrahepatic tissues, such as brain, pancreas, and breast cancer cells, as well as many other cell types (29). GLS2 localizes to the inner mitochondrial membrane to catalyze the hydrolysis of the γ-amino group of GLN forming glutamate and ammonia (27). This ammonia may be used to form carbamoyl phosphate or may diffuse from the mitochondria and the cell. Glutamate can be further deaminated to form α-ketoglutarate and thus enter the citric acid cycle for energy metabolism. Glutamate also preserves total GSH levels after oxidative stress (22, 30). Our data indicate that p53-inducible GLS2 regulates intracellular glutamine metabolism and ROS levels and promotes antioxidant defense through controlling the GSH/GSSG ratio, although we do not exclude the additional possibility that regeneration of GSH from GSSG is increased by *GLS2* expression.

The modulation of intracellular ROS levels in cells is important in controlling the development and maintenance of tumors. A number of p53-induced antioxidant genes have been previously reported, including sestrins (*SESN1* and *SESN2*) (31), aldehyde dehydrogenase 4 (*ALDH4*) (32), and *TIGAR* (14). Sestrins (SENS1 and SENS2) are essential for regulation of overoxidized peroxiredoxins (31). TIGAR blocks glycolysis, leading to elevated NADPH generation that results in increased GSH levels, thus promoting consumption of ROS (8). ALDH4 is a mitochondrial-matrix NAD+-dependent enzyme converting L-glutamic-γ-semialdehyde to glutamate via the proline degradation pathway (32). Here we have identified another metabolic role for p53 in the control of glutamine metabolism through GLS2. It is interesting that the activities of TIGAR, ALDH4, and GLS2 proteins converge onto a common mechanism in their regulation of intracellular ROS levels.

Recently, several studies have shown that p53 has a role in the regulation of both glycolysis and oxidative phosphorylation. p53 slows glycolysis by inhibiting the expression of the glucose trans-

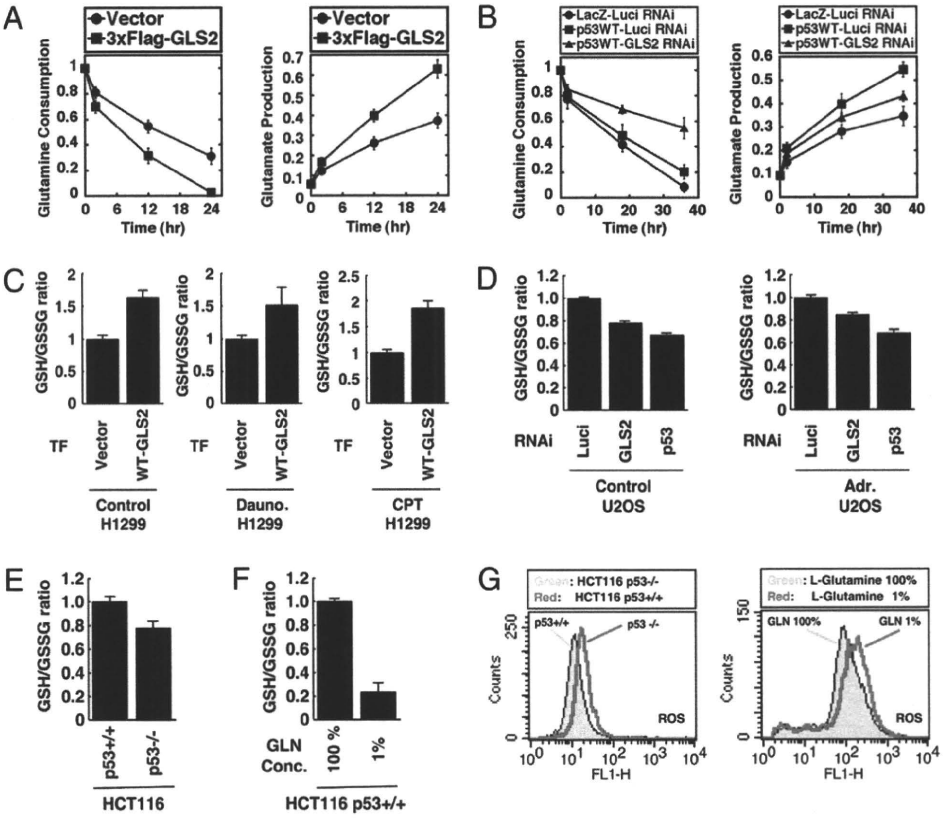

Fig. 3. GLS2 controls glutamine metabolism and GSH antioxidant capacity to decrease intracellular ROS levels. (*A*) Cells were transfected with indicated plasmids for 24 h and then switched to fresh medium. Glutamine consumption is represented as a ratio to initial concentration and graphs show the mean of six measurements from two independent experiments, with error bars representing SD. (*B*) Cells were transfected with luciferase RNAi (closed circles and squares) or GLS2 RNAi (closed triangles) for 12 h and then cells were infected with adenoviruses expressing either LacZ or WT p53 (p53WT) at a multiplicity of infection of 2 for another 24 h. Cultures were switched to fresh medium and glutamine consumption and glutamate production was calculated as in *A*. (*C*) Cells were transfected with indicated plasmids for 48 h. After the selection in the presence of 600 μg/mL G418 for 5 d, cells were split and cultured for 24 h, and then not treated (control) or treated with daunorubicin or CPT for another 24 h. Cells were collected and subjected to GSH and GSSG assay as described in *Materials and Methods*. Graphs show the mean of two independent experiments, with error bars representing SD. (*D*) Cells were transfected with indicated RNAi for 24 h and then either not treated (control; *Left*) or treated with doxorubicin (100 nM; *Right*) for another 24 h. Cells were collected and subjected to GSH and GSSG assay as in *C*. (*E*) HCT116 cells that either express p53 ($p53^{+/+}$) or lack p53 ($p53^{-/-}$) were cultured exponentially and then subjected to GSH and GSSG assay as in *C*. (*F*) HCT116 ($p53^{+/+}$) cells were cultured exponentially and then switched to normal medium containing 100% (584 mg/L) L-glutamine (GLN), or glutamine depletion medium containing 1% (5.8 mg/L) GLN, and then cultured for 36 h. Assay of GSH and GSSG was performed as in *C*. (*G*) HCT116 cells that either express p53 ($p53^{+/+}$) or lack p53 ($p53^{-/-}$) were cultured exponentially (*Left*) or HCT116 $p53^{+/+}$ cells were switched to normal medium (GLN; 100%) or glutamine depletion medium (GLN; 1%) for 36 h as in *F*. DCF staining was followed by FACS analysis.

porters GLUT1, GLUT4, and GLUT3 and decreasing the levels of phosphoglycerate mutase (PGM) while increasing the expression of *TIGAR*. However, these findings are confounded by other studies showing apparently opposing activities: for example, the presence of p53-responsive elements in the promoters of *PGM* and *hexokinase II* suggests that p53 can promote at least some steps in glycolysis (3). Another study has shown that p53 induces expression of SCO2 (synthesis of cytochrome *c* oxidase 2) that participates in the assembly of cytochrome *c* oxidase (COX) in mitochondria, implicating p53 in the regulation of oxygen consumption and mitochondrial respiration (14). Similar to SCO2, GLS2 expression may cause subsequent metabolic changes in mitochondrial respiration as its glutamate product can eventually be further deaminated to form α-ketoglutarate and thus enter the TCA cycle. Indeed, the overexpression of GLS2 increased ATP production in H1299 cells whereas GLS2 silencing inhibited ATP levels in U2OS cells (Fig. S9). These findings connecting p53 to the regulation of energy production are rather complicated, and it is very likely that the roles of p53 in responding to and effecting alterations in metabolism will have consequences beyond cancer, influencing other aspects of normal life and disease. Future investigations should provide more information as to how p53 is able to coordinate the actions of multiple intracellular metabolic networks to exert its tumor suppressive function.

During oncogenesis, as cells accumulate defects in the p53 pathway, multiple intracellular metabolic safety mechanisms are bypassed. Energy supply and consumption systems, including glutamine metabolism and glycolysis, proceed at full capacity and the normal restraints on tumor growth are lost. It is thus possible that GLS2 expression might be under positive selection in tumors as a result of GLS2's control of energy metabolism. Indeed, it was shown that GLS activity is positively correlated with malignancy in tumors (23). Recently, it was shown that c-Myc up-regulates GLS1 through its ability to repress miR-23a and miR-23b (33). These data seem to be at odds with our findings that p53 may be supplying the TCA cycle through its related target, GLS2. As both enzymatic forms of GLS have distinct kinetic and molecular characteristics (34), we speculate that the differential regulation of GLS1 and GLS2 may reflect their possibly distinct functions or requirements in different tissues or cell states (33).

Finally, we have demonstrated that GLS2 reduces cellular sensitivity to ROS-associated apoptosis possibly through GSH-dependent antioxidant defense processes. Yet it was shown that increased ROS levels lead to stabilized and activated p53 (35).

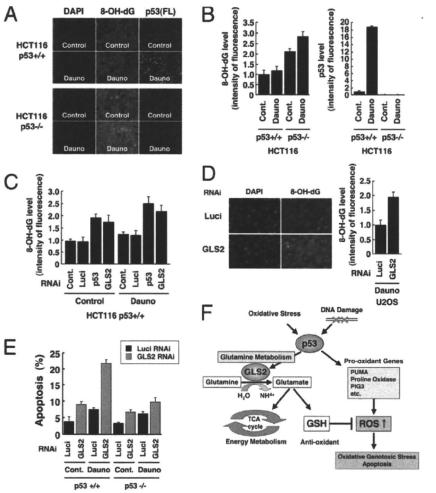

Fig. 4. p53 and GLS2 regulate DNA oxidation and ROS-mediated apoptosis. (*A*) HCT116 cells were untreated (control) or treated with daunorubicin (Dauno.; 100 nM) for 24 h and then fixed and stained using anti-8-OH-dG antibody and anti-p53 polyclonal antibody (FL) and visualized using Alexa Fluor–488– and -594–conjugated secondary antibodies. Nuclei were counterstained with DAPI and images were taken using a Keyence microscope. (*B*) HCT116 cells were treated as in *A*. Intensity of 8-OH-dG (*Left*) and p53 (*Right*) staining was quantified using Keyence software. The average of six random visual fields from two independent experiments is shown, with error bars representing SD. (*C*) HCT116 cells expressing WT p53 ($p53^{+/+}$) were transfected with indicated RNAi for 24 h and then cells were either not treated (untreated) or treated with daunorubicin (100 nM) for another 24 h. DNA oxidation was detected as in *A* and quantified as in *B*. (*D*) U2OS cells were transfected with luciferase RNAi or GLS2 RNAi and then treated with daunorubicin (100 nM) as in *C*. DNA oxidation was detected and quantified as in *C*. (*E*) HCT116 ($p53^{+/+}$) or ($p53^{-/-}$) cells were transfected with luciferase RNAi (Luci) or GLS2 RNAi for 24 h and then were either not treated (control) or treated with daunorubicin (300 nM) for another 36 h. The amount of sub–G0/G1 cells was calculated using the Cell Quest program for FACS. Average of three independent experiments is shown, with error bars indicating SD. (*F*) Model for regulation of intracellular ROS levels by GLS2. Upon oxidative stress or DNA damage, p53 is stabilized and activated to induce several targets including antioxidant and prooxidant genes. One such target, GLS2, catalyzes the hydrolysis of glutamine to produce glutamate and NH4+ and functions as an antioxidant protein. In response to severe cellular stress or irreparable damage p53 transactivates prooxidant genes (*PUMA, PIG3, Proline Oxidase*), resulting in the elevation of intracellular ROS, and apoptosis. The balance between anti- and prooxidant genes and the differential regulation of p53 targets can determine the choice of cellular outcomes.

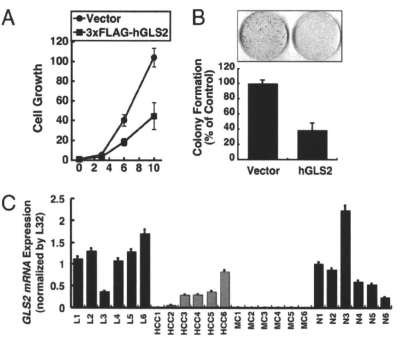

Fig. 5. GLS2 inhibits tumor cell growth and colony formation and GLS2 expression is decreased in liver tumors. (*A*) Cells were transfected as indicated for 48 h. Cells were then split and subjected to the cell growth analysis (*Left*) or colony formation assay visualized by crystal violet staining (*Right*). (*B*) Loss or reduction of GLS2 mRNA expression in human liver tumors. N, normal liver; L, tumor adjacent tissues with chronic hepatitis; HCC, hepatocellular carcinoma; MC, liver-metastatic tumor of colorectal carcinomas. The expression of GLS2 mRNA were determined by real-time PCR and normalized by actin expression.

As we cannot exclude the possibility that GLS2 expression affects certain p53 target gene(s) or some specific function of p53, which leads to the modulation of ROS-associated apoptosis, further investigation is required to clarify the relationship among ROS levels, glutamine metabolism, and p53-dependent apoptotic response. At present, the duality of p53 function as an inducer of antioxidant genes, including *GLS2* and *TIGAR*, while also activating genes that enhance oxidative stress, remains to be elucidated. Perplexingly, both antioxidant and prooxidant outcomes of p53 transcription are proposed to contribute to tumor suppression. Nevertheless, our results that GLS2 inhibits tumor cell growth and is underexpressed in liver tumors implicate GLS2 as a contributor to p53-mediated tumor suppression and should provide impetus for further studies on this topic.

Materials and Methods

Cell Lines, Cell Culture, Western Blot Analysis, and Antibodies. For detailed description of cell lines and antibodies, immunoblotting, real-time RT-PCR, FACS, and colony formation assays, please refer to *SI Materials and Methods*.

Chromatin Immunoprecipitation Assay. H1299 cells infected with a recombinant adenovirus expressing p53 (Ad-p53; 30 MoI) and HCT116 cells ($p53^{+/+}$ and $p53^{-/-}$) were treated with daunorubicin (220 nM) for 24 h. Then cells were prepared for ChIP analysis. See *SI Materials and Methods* for a detailed protocol.

Preparation of Mitochondria. The mitochondrial fraction was prepared as previously described (36). A detailed protocol is described in *SI Materials and Methods*.

RNA Interference. siRNA oligonucleotides whose sequences are listed in *SI Materials and Methods* were synthesized by Qiagen. HCT116 cells ($p53^{+/+}$ and $p53^{-/-}$), U2OS cells, and HEAC cells were plated at 50% confluence and transfected with the indicated siRNA oligonucleotide (50 nM) using Dharmafect 1 (Dharmacon). Twenty-four hours later the cells were left untreated or exposed to daunorubicin, H_2O_2, or different drugs as indicated in the figure legends for 24 h before analysis.

Measurement of ROS. Cells were incubated with 3 μM 2′,7′-dichlorodihydrofluorescein diacetate (DCF; Molecular Probes) for 15 min at 37 °C. After incubation, cells were washed with PBS, trypsinized, and resuspended in PBS solution, and fluorescence was measured using a FACScan flow cytometer (excitation at 488 nm, emission at 515–545 nm) and data analyzed with CELL Quest software.

Glutathione Assay. Total GSH and GSSG were measured with the glutathione quantification kit (Dojindo). In brief, the deproteinated sample was used to determine GSH content via a standard enzymatic recycling procedure. To determine the GSSG content, an aliquot of the deproteinated supernatant was mixed with 2-vinyl-pyridine (Sigma-Aldrich) and triethanolamine (Sigma-Aldrich) and then assayed.

Determination of Glutamate and Glutamine Concentrations. Concentrations of glutamate and glutamine in the medium were determined using a glutamine/glutamate determination kit (GLN-1; Sigma-Aldrich). The determination of L-glutamine was done in a two-step reaction: (*i*) deamination of L-glutamine to

L-glutamate and (*ii*) dehydrogenation of the L-glutamate to α-ketoglutarate accompanied by reduction of NAD+ to NADH. The conversion of NAD+ to NADH was measured using a spectrophotometer at 340 nm. The amount of NADH is proportional to the amount of glutamate. A standard curve was determined for each day the samples were run to calculate the concentration of glutamate in the sample.

ACKNOWLEDGMENTS. We are grateful to Professor Yasushi Saito and Naoko Hashimoto for helpful suggestions and discussions throughout this work. We thank Kayo Suzuki and Takako Hatada for expert technical assistance. This work was supported by National Institutes of Health Grants CA77742 and CA87497, the Global COE Program (Global Center for Education and Research in Immune System Regulation and Treatment); MEXT (Japan); Grants-in-Aid from the Ministry of Education, Culture, Sports, Science and Technology (Japan) for Scientific Research on Priority Areas 17016010 and 20012010, Scientific Research (B) 21390147 and (C) 19659121, and Exploratory Research and Young Scientists (B) 20790367; the Tokyo Biochemical Research Foundation, the Sumitomo Foundation; the Mochida Memorial Foundation; the Takeda Science Foundation; the Sankyo Foundation of Life Science; and the Japan Diabetes Foundation.

1. Deberardinis RJ, Sayed N, Ditsworth D, Thompson CB (2008) Brick by brick: metabolism and tumor cell growth. *Curr Opin Genet Dev* 18:54–61.
2. Kroemer G, Pouyssegur J (2008) Tumor cell metabolism: cancer's Achilles' heel. *Cancer Cell* 13:472–482.
3. Vousden KH, Ryan KM (2009) p53 and metabolism. *Nat Rev Cancer* 9:691–700.
4. Warburg O (1956) On the origin of cancer cells. *Science* 123:309–314.
5. Vander Heiden MG, Cantley LC, Thompson CB (2009) Understanding the Warburg effect: the metabolic requirements of cell proliferation. *Science* 324:1029–1033.
6. Schwartzenberg-Bar-Yoseph F, Armoni M, Karnieli E (2004) The tumor suppressor p53 down-regulates glucose transporters GLUT1 and GLUT4 gene expression. *Cancer Res* 64:2627–2633.
7. Kondoh H, et al. (2005) Glycolytic enzymes can modulate cellular life span. *Cancer Res* 65:177–185.
8. Bensaad K, et al. (2006) TIGAR, a p53-inducible regulator of glycolysis and apoptosis. *Cell* 126:107–120.
9. Mathupala SP, Ko YH, Pedersen PL (2006) Hexokinase II: cancer's double-edged sword acting as both facilitator and gatekeeper of malignancy when bound to mitochondria. *Oncogene* 25:4777–4786.
10. Ruiz-Lozano P, et al. (1999) p53 is a transcriptional activator of the muscle-specific phosphoglycerate mutase gene and contributes in vivo to the control of its cardiac expression. *Cell Growth Differ* 10:295–306.
11. Kulawiec M, Ayyasamy V, Singh KK (2009) p53 regulates mtDNA copy number and mitocheckpoint pathway. *J Carcinog* 8:8.
12. Lebedeva MA, Eaton JS, Shadel GS (2009) Loss of p53 causes mitochondrial DNA depletion and altered mitochondrial reactive oxygen species homeostasis. *Biochim Biophys Acta* 1787:328–334.
13. Okamura S, et al. (1999) Identification of seven genes regulated by wild-type p53 in a colon cancer cell line carrying a well-controlled wild-type p53 expression system. *Oncol Res* 11:281–285.
14. Matoba S, et al. (2006) p53 regulates mitochondrial respiration. *Science* 312: 1650–1653.
15. Bourdon A, et al. (2007) Mutation of RRM2B, encoding p53-controlled ribonucleotide reductase (p53R2), causes severe mitochondrial DNA depletion. *Nat Genet* 39: 776–780.
16. Reitzer LJ, Wice BM, Kennell D (1979) Evidence that glutamine, not sugar, is the major energy source for cultured HeLa cells. *J Biol Chem* 254:2669–2676.
17. Pérez-Gómez C, et al. (2005) Co-expression of glutaminase K and L isoenzymes in human tumour cells. *Biochem J* 386:535–542.
18. Kvamme E, Nissen-Meyer LS, Roberg BA, Torgner IA (2008) Novel form of phosphate activated glutaminase in cultured astrocytes and human neuroblastoma cells, PAG in brain pathology and localization in the mitochondria. *Neurochem Res* 33:1341–1345.
19. Sablina AA, et al. (2005) The antioxidant function of the p53 tumor suppressor. *Nat Med* 11:1306–1313.
20. Bensaad K, Vousden KH (2007) p53: new roles in metabolism. *Trends Cell Biol* 17: 286–291.
21. Sies H (1999) Glutathione and its role in cellular functions. *Free Radic Biol Med* 27: 916–921.
22. Matés JM, Pérez-Gómez C, Núñez de Castro I, Asenjo M, Márquez J (2002) Glutamine and its relationship with intracellular redox status, oxidative stress and cell proliferation/death. *Int J Biochem Cell Biol* 34:439–458.
23. Lora J, et al. (2004) Antisense glutaminase inhibition decreases glutathione antioxidant capacity and increases apoptosis in Ehrlich ascitic tumour cells. *Eur J Biochem* 271:4298–4306.
24. Ogunlesi F, Cho C, McGrath-Morrow SA (2004) The effect of glutamine on A549 cells exposed to moderate hyperoxia. *Biochim Biophys Acta* 1688:112–120.
25. Jackson AL, Loeb LA (2001) The contribution of endogenous sources of DNA damage to the multiple mutations in cancer. *Mutat Res* 477:7–21.
26. Green DR, Chipuk JE (2006) p53 and metabolism: Inside the TIGAR. *Cell* 126:30–32.
27. Kovacevic Z, McGivan JD (1983) Mitochondrial metabolism of glutamine and glutamate and its physiological significance. *Physiol Rev* 63:547–605.
28. Watford M (1993) Hepatic glutaminase expression: relationship to kidney-type glutaminase and to the urea cycle. *FASEB J* 7:1468–1474.
29. Gómez-Fabre PM, et al. (2000) Molecular cloning, sequencing and expression studies of the human breast cancer cell glutaminase. *Biochem J* 345:365–375.
30. Yudkoff M, et al. (1990) Glutathione turnover in cultured astrocytes: studies with [15N]glutamate. *J Neurochem* 55:137–145.
31. Budanov AV, Sablina AA, Feinstein E, Koonin EV, Chumakov PM (2004) Regeneration of peroxiredoxins by p53-regulated sestrins, homologs of bacterial AhpD. *Science* 304: 596–600.
32. Yoon KA, Nakamura Y, Arakawa H (2004) Identification of ALDH4 as a p53-inducible gene and its protective role in cellular stresses. *J Hum Genet* 49:134–140.
33. Gao P, et al. (2009) c-Myc suppression of miR-23a/b enhances mitochondrial glutaminase expression and glutamine metabolism. *Nature* 458:762–765.
34. Curthoys NP, Watford M (1995) Regulation of glutaminase activity and glutamine metabolism. *Annu Rev Nutr* 15:133–159.
35. Chen K, Albano A, Ho A, Keaney JF, Jr (2003) Activation of p53 by oxidative stress involves platelet-derived growth factor-beta receptor-mediated ataxia telangiectasia mutated (ATM) kinase activation. *J Biol Chem* 278:39527–39533.
36. Trounce A, Kim YL, Jun AS, Wallace DC (1996) Assessment of mitochondrial oxidative phosphorylation in patient muscle biopsies, lymphoblasts, and transmitochondrial cell lines. *Methods Enzymol* 264:484–494.

Arteriosclerosis, Thrombosis, and Vascular Biology

JOURNAL OF THE AMERICAN HEART ASSOCIATION

American Heart Association®

Learn and Live℠

CCN3 Inhibits Neointimal Hyperplasia Through Modulation of Smooth Muscle Cell Growth and Migration

Tatsushi Shimoyama, Shûichi Hiraoka, Minoru Takemoto, Masaya Koshizaka, Hirotake Tokuyama, Takahiko Tokuyama, Aki Watanabe, Masaki Fujimoto, Harukiyo Kawamura, Seiya Sato, Yuya Tsurutani, Yasushi Saito, Bernard Perbal, Haruhiko Koseki and Koutaro Yokote

Arterioscler Thromb Vasc Biol 2010;30;675-682; originally published online Feb 5, 2010;
DOI: 10.1161/ATVBAHA.110.203356
Arteriosclerosis, Thrombosis, and Vascular Biology is published by the American Heart Association. 7272 Greenville Avenue, Dallas, TX 72514
 Print ISSN: 1079-5642. Online ISSN: 1524-4636

CCN3 Inhibits Neointimal Hyperplasia Through Modulation of Smooth Muscle Cell Growth and Migration

Tatsushi Shimoyama, Shûichi Hiraoka, Minoru Takemoto, Masaya Koshizaka, Hirotake Tokuyama, Takahiko Tokuyama, Aki Watanabe, Masaki Fujimoto, Harukiyo Kawamura, Seiya Sato, Yuya Tsurutani, Yasushi Saito, Bernard Perbal, Haruhiko Koseki, Koutaro Yokote

Objective—*CCN3* belongs to the CCN family, which constitutes multifunctional secreted proteins that act as matrix cellular regulators. We investigated the pathophysiological roles of *CCN3* in the vessels.

Methods and Results—We examined the effects of *CCN3* on the proliferation and migration of rat vascular smooth muscle cells (VSMC). *CCN3* knockout mice were created, and vascular phenotypes and neointimal hyperplasia induced by photochemically induced thrombosis were investigated. *CCN3* suppressed the VSMC proliferation induced by fetal bovine serum. The neutralizing antibody for transforming growth factor-β did not affect the growth inhibitory effect of *CCN3*. Moreover, *CCN3* enhanced the mRNA expression of cyclin-dependent kinase inhibitors, p21 and p15. Gamma secretase inhibitor, an inhibitor of Notch signaling, partially inhibited the enhanced expression of p21 induced by *CCN3*. *CCN3* also inhibited the VSMC migration. Finally, the histopathologic evaluation of the arteries 21 days after the endothelial injury revealed a 6-fold enhancement of neointimal thickening in the null mice compared with the wild-type mice.

Conclusion—*CCN3* suppresses neointimal thickening through the inhibition of VSMC migration and proliferation. Our findings indicate the involvement of *CCN3* in vascular homeostasis, especially on injury, and the potential usefulness of this molecule in the modulation of atherosclerotic vascular disease. (***Arterioscler Thromb Vasc Biol.* 2010;30:675-682.)**

Key Words: growth factors ■ vascular biology ■ vascular muscle

CCN3/NOV belongs to a family of multicellular growth regulators originally referred to as the acronym CCN (cysteine-rich protein, Cyr 61/*CCN1*; connective tissue growth factor, CTGF/*CCN2*; and nephroblastoma overexpressed, NOV/*CCN3*), which now includes 3 additional genes (Wnt-1–induced secreted proteins 1 to 3; *WISP1–3/CCN4–6*).[1,2] The *CCN3* gene was first isolated from avian nephroblastomas induced by viral infections.[3] Its antiproliferative activity in a variety of cells is now well-established, especially in tumor cells.[4,5]

See accompanying article on page 667

Although other members of the CCN family, such as *CCN1* and *CCN2*, are strongly expressed in a wide range of tissues,[6,7] *CCN3* mRNA is highly and restrictively expressed in rat aortas and carotid arteries.[8] This specific expression pattern in vessels indicates that *CCN3* plays an important role in vascular homeostasis.

This article accompanies the DVT Series that was published in the March 2010 issue.

The knockdown of *CCN1*/Cyr61 in mice suppresses neointimal hyperplasia in a rat artery balloon injury model.[9] *CCN2*/CTGF also accumulates in the shoulders of human rupture-prone atherosclerotic plaques.[10] Because CTGF induces mononuclear cell chemotaxis in a dose-dependent manner in vitro, CTGF may also have a role in atherogenesis. However, despite the similarity of the amino acid sequence of *CCN3* and *CCN1* and *CCN2*,[4] the pathophysiological roles of *CCN3* in vessels has not been fully elucidated. The present study confirmed the expression of *CCN3* in medial layer of mouse aortas. Therefore, the effects of *CCN3* on vascular smooth muscle cell (VSMC) proliferation and migration were investigated. Finally, *CCN3*-null mice were created and the physiological and pathological roles of *CCN3* in vessels were determined.

Received on: November 29, 2009; final version accepted on: January 14, 2009.

From Department of Clinical Cell Biology and Medicine (T.S., M.K., H.T., T.T., A.W., H.K., Y.T., K.Y.), Chiba University Graduate School of Medicine, Chiba, Japan; Department of Regenerative Medicine (S.H.), National Research Institute for Child Health and Development, Tokyo, Japan; Department of Medicine (M.T., M.F., K.Y.), Division of Diabetes, Metabolism, and Endocrinology, Chiba University Hospital, Chiba, Japan; Seiwa Narashino (S.S.), Chiba, Japan; Chiba University (Y.S.), Chiba, Japan; Laboratoire d'Oncologie Virale et Moléculaire (B.P.), Université Paris, Paris, France; RIKEN Research Center for Allergy and Immunology (H.K.), Yokohama, Japan.

T.S. and S.H. contributed equally to this work.

Correspondence to Minoru Takemoto, Department of Medicine, Division of Diabetes, Metabolism and Endocrinology, Chiba University Hospital, Chiba, Japan, 1-8-1 Inohana, Chuo-ku, Chiba 260-8670, Japan. E-mail minoru.takemoto@faculty.chiba-u.jp or Haruhiko Koseki, Developmental Genetics, RIKEN Research Center for Allergy and Immunology (RCAI), RIKEN Yokohama Institute, 1-7-22 Suehiro, Tsurumi-ku, Yokohama 230-0045, Japan. E-mail koseki@rcai.riken.jp

Arterioscler Thromb Vasc Biol **is available at http://atvb.ahajournals.org** **DOI: 10.1161/ATVBAHA.110.203356**

Materials and Methods

Reagents

The reagents used are described in the expanded Supplementary Materials and Methods section (available online at http://atvb.ahajournals.org).

Cell Culture

Primary cultures of rat aortic smooth muscle cells were isolated from 250- to 300-gram Wister Rats (QLEA Japan, Inc.) as described previously.[11] See the Supplementary Materials and Methods section for details.

Semiquantitative Reverse-Transcription Polymerases Chain Reaction

Reverse-transcription polymerase chain reaction is described in the Supplementary Materials and Methods section.

Proliferation Assay

VSMC proliferation was quantified by direct cell counting and by 5-bromo-2′-deoxyuridine (BrdU) incorporation using a commercially available enzyme-linked immunosorbent assay kit (Roche Diagnostics). See the Supplementary Materials and Methods section for details.

Migration Assay

The ability of smooth muscle cells to migrate toward *CCN3* was examined using a 96-well chemotaxis chamber (AB96; Neuro Probe).[12] See the Supplementary Materials and Methods section for details.

Western Blotting

Western blotting was performed essentially as described previously.[13] See the Supplementary Materials and Methods section for details.

Generation of *CCN3* Mutant Mice

A knockout mouse line of the *CCN3* gene was generated according to methods previously described.[14] See the Supplementary Materials and Methods section for details.

Genotyping of Mutant Mice

Genomic southern hybridization and polymerase chain reaction were used to determined the *CCN3* genotype (Supplementary Figure IVA, IVB available online at http://atvb.ahajournals.org) using genomic DNA extracted from embryo stem cells and tails, according to methods previously described.[14] See the Supplementary Materials and Methods section for details.

Induction of Diabetes

Diabetes was induced by the injection of streptozotocin. See the Supplementary Materials and Methods section for details.

Immunohistochemistry and Immunocytochemistry

Immunohistochemistry and immunocytochemistry are described in the Supplementary Materials and Methods section.

Femoral Artery Injury

Mice femoral arteries were injured by means of a photochemically induced thrombosis method.[15] See the Supplementary Materials and Methods section for details.

Statistical Analysis

All values are expressed as the mean±SD. The statistical significance was evaluated using the unpaired Student *t* test. $P<0.05$ was considered to be significant.

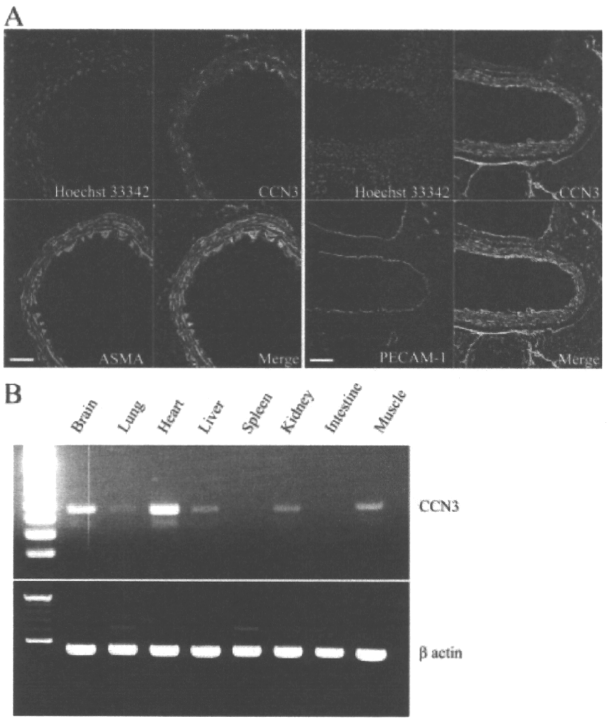

Figure 1. The expression of *CCN3* in mouse aortas and different mouse tissues. A, The expression of *CCN3* in the aorta of 2-month-old mice was examined by immunohistochemistry using anti-*CCN3*–specific antibody and compared with the expression of anti-alpha smooth muscle actin, as well as anti-platelet endothelial cell adhesion molecule-1. Bars=50 μm. B, Total RNA were isolated from the various tissues of 2-week-old mice and *CCN3* mRNA expression was compared by reverse-transcription polymerase chain reaction.

Results

Expression of *CCN3* Protein in Mouse Aorta and Distribution of *CCN3* Gene Expression in Mouse Tissues

First, we determined the expression of the *CCN3* protein in the mouse aortas by immunohistochemistry using the anti-*CCN3*-specific antibody. The anti-alpha smooth muscle actin antibody was used as a marker for VSMC and anti-platelet endothelial cell adhesion molecule-1 (PECAM-1) antibody was used as a marker for endothelial cells. The *CCN3* protein was localized in the medial layer of the mouse aorta and colocalized with anti-alpha smooth muscle actin-positive cells but not with anti-PECAM-1-positive cells (Figure 1A). Next, we examined the expression of *CCN3* in different mouse tissues by using reverse-transcription polymerase chain reaction. As shown in Figure 1B, the expression of *CCN3* mRNA was the highest in the heart, weak in the brain, lung, and muscle tissues, and absent in the spleen and intestine.

CCN3 Inhibits VSMC Proliferation Independent of TGF-β Signaling and VSMC Migration

The expression of *CCN3* mRNA was examined in cultured rat VSMC. *CCN3* mRNA was detected in rat VSMC and increased with time in culture (Supplementary Figure IA).

Next, the biological functions of *CCN3* were examined in cultured VSMC. Because *CCN3* has antiproliferative activities in several tumor cell lines, we used human recombinant *CCN3* proteins to determine whether *CCN3* also inhibited VSMC proliferation in vitro. VSMC were plated in culture dishes in the presence or absence of 100 ng/mL *CCN3* and the number of cells was counted every day. The number of VSMC was significantly lower in the presence of *CCN3* from day 2 until day 4 after the start of the culture. However, this difference disappeared once the VSMC reached confluence (Supplementary Figure IB). The antiproliferative activity of *CCN3* was also evaluated using BrdU incorporation. *CCN3* alone had no effect on VSMC proliferation. However, *CCN3* significantly inhibited VSMC proliferation induced by 10% fetal bovine serum (FBS), as well as that by platelet-derived growth factor-BB (PDGF-BB), in a dose-dependent manner (Figure 2A). Further, we also examined the effects of *CCN3* on the cell cycle by flow cytometric analysis. The VSMC were treated with FBS in the presence of CCN3 or TGF-b and labeled with propidium iodide (PI). The ratio of PI-labeled smooth muscle cells in the G2/M phase to those in the G0/G1 phase was significantly decreased after both CCN3 and TGF-b treatment (Supplementary Figure IC, ID). In addition, the Trypan blue exclusion test was used to confirm that *CCN3* was not toxic to cells (data not shown).

TGF-β inhibits the proliferation of a variety of cell types.[16] Therefore, we examined whether TGF-β is involved in the inhibition of VSMC proliferation by *CCN3*. A TGF-β–specific neutralizing antibody was used to inhibit TGF-β. Both *CCN3* and TGF-β inhibited the VSMC proliferation induced by 10% fetal bovine serum. An anti-TGF-β–specific neutralizing antibody could reverse the antiproliferative effects induced by TGF-β, but not those induced by *CCN3*. The anti-TGF-β–specific neutralizing antibody alone had no effects on VSMC proliferation (Figure 2B). Moreover, *CCN3* also inhibited the VSMC migration induced by FBS in a dose-dependent manner (Figure 2C).

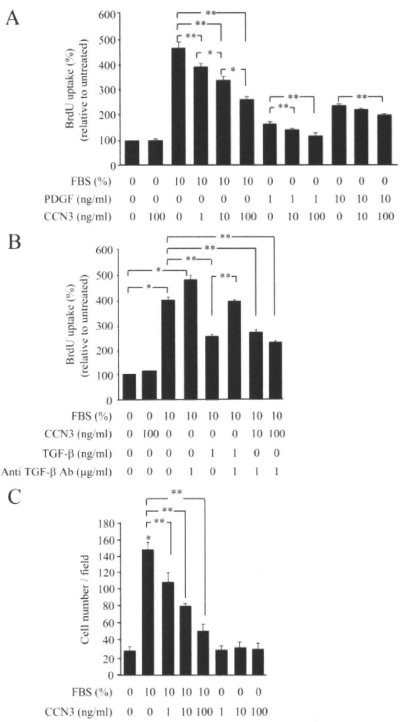

Figure 2. Effects of recombinant *CCN3* on VSMC proliferation and migration. A and B, Cells were serum-starved for 24 hours and then incubated with the indicated concentrations of fetal bovine serum, platelet-derived growth factor-BB, *CCN3*, TGF-β, and anti-TGF-β antibody in the presence of BrdU at 37°C for 24 hours. BrdU incorporation was then determined by enzyme-linked immunosorbent assay and compared with the controls. C, The effects of various doses of *CCN3* on VSMC migration were measured using a modified Boyden chamber method. Representative results of 3 independent experiments are presented. Bars represent the mean±SD *$P<0.05$, **$P<0.01$.

CCN3 Increases the Expression of the CDK Inhibitors p15 and p21 Through the Notch Signaling Pathway

We examined the expression of cell cycle regulators to determine the molecular mechanism underlying the antiproliferative activity of *CCN3*. Among the factors studied, both *CCN3* and TGF-β upregulated the cyclin-dependent kinase inhibitors p15 and p21 within 12 hours (Figure 3A). A time-course study revealed that *CCN3* treatment increased the expression of p21 mRNA after 12 hours, but the expression returned to the baseline within 24 hours, whereas TGF-β treatment increased the expression of p21 mRNA in a time-dependent manner (Supplementary Figure IE). This result supported the idea that *CCN3* increases the expression of cell-cycle regulators independently of TGF-β signaling. The effects of *CCN3* on TGF-β signaling were also examined. *CCN3* had little effect on either the phosphorylation of *Smad2* (Figure 3B) or the activation of plasminogen activator inhibitor-1 (PAI-1) promoter, which contains the TGF-β–responsive element (Supplementary Figure IF). Collectively, these data indicated that *CCN3* inhibited VSMC proliferation independent of TGF-β signaling.

CCN3 activates the Notch signaling pathway through its carboxyl-terminal cysteine-rich domain and inhibits osteogenic differentiation and cell proliferation in Kusa-A1 cells.[17] Therefore, the effects of *CCN3* on the Notch pathway in VSMC were examined. First, we examined the effect of both TGF-β and *CCN3* on the expression of the intracellular domain of Notch1 (ICN1). This domain is proteolytically cleaved from the plasma membrane in conjunction with the activation of the Notch receptor. The

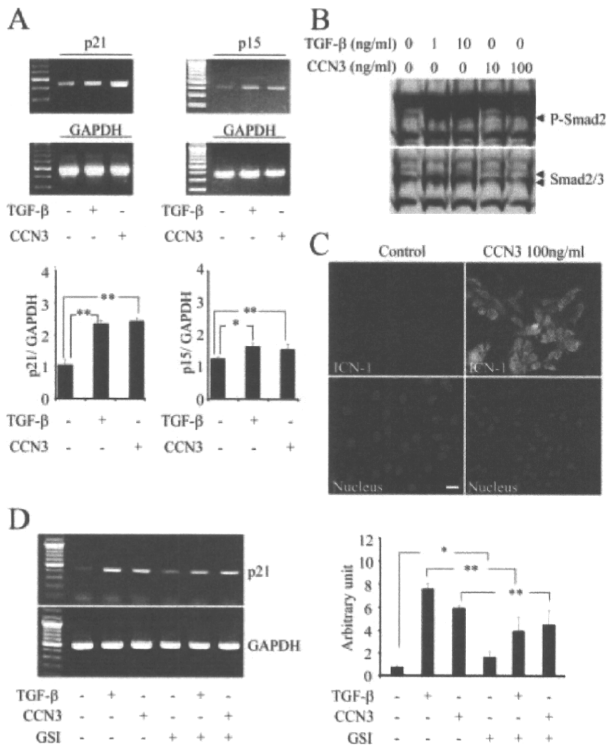

Figure 3. *CCN3* upregulated the expression of cell cycle regulators, *p15* and *p21*, through the Notch signaling pathway. A, Cells were serum-starved for 24 hours and then incubated with 1 ng/mL TGF-β_1 or 100 ng/mL *CCN3* for 12 hours at 37°C. Then, the expressions of *p21* and *p15* were examined and compared with the expression of GAPDH by reverse-transcription polymerase chain reaction. B, The expressions of phospho-*Smad2* and total *Smad2/3* were determined by immunoblotting. C, The expression of ICN1 was examined by immunohistochemistry. Bars=20 μm. D, The cells were incubated with 1 ng/mL TGF-β_1 or 100 ng/mL *CCN3* in the presence or absence of 5 μmol/L γ-secretase inhibitor for 12 hours. The expression of *p21* was examined and compared with the expression of GAPDH by reverse-transcription polymerase chain reaction. One representative experiment out of 2 is shown.

antibody (Val 1774) that we used could recognize cleaved ICN1 but could not recognize uncleaved ICN1. Therefore, once the Notch pathway was activated, we were able to observe the ICN1 protein in the cells by immunocytochemistry. *CCN3* increased ICN1 expression in the VSMC within 30 minutes (Figure 3C), whereas TGF-β had little effect (data not shown). Next, we investigated the effect of a γ-secretase inhibitor, which blocks the Notch signaling pathway not only during VSMC proliferation but also during *p21* regulation. γ-Secretase inhibitor reversed the *CCN3*-dependent antiproliferative effects of VSMC, which had been evaluated using BrdU incorporation (Supplementary Figure IIA). γ-Secretase inhibitor alone slightly increased the expression of *p21*. However, the upregulation of *p21* expression by both *CCN3* and TGF-β was partially but significantly suppressed by γ-secretase inhibitor treatment (Figure 3D). We also examined the effects of RPMS-1, a known blocker of the RBP-J–mediated Notch signaling pathway, on the effects of *CCN3*. As shown in Supplementary Figure IIB, the expression of *Hey1*, a gene targeted by the Notch signal, increased in the presence of *CCN3*. The overexpression of RPMS-1 in the VSMC inhibited the *CCN3*-induced expression of *Hey1*. The increase in the expression of *p21* mRNA induced by *CCN3* was suppressed by the overexpression of RPMS-1. These results indicated that *CCN3*/Notch is a signaling pathway that increases the expression of the cell-cycle regulators. Recently it has been reported that PDGF receptor-β is a direct target of the activated Notch1 and Notch3 receptors.[18] Therefore, we examined the effects of *CCN3* on the expression of PDGF receptor-β and its tyrosine phosphorylation and ERK activation in VSMC. None of these responded to *CCN3*, as shown in Supplementary Figure IIIA and IIIB.

Mice Lacking *CCN3* Show Enhanced Neointimal Hyperplasia in Response to Injury

CCN3$^{-/-}$ mice were generated by conventional homologous recombination to investigate the physiological and pathological roles of *CCN3* in vivo. Bacterial artificial chromosome-based targeting vectors were used to specifically replace exons 1, 2, and a part of exon 3 of the *CCN3* gene with a neomycin selection cassette (Figure 4A). Chimeric mice derived from embryo stem cell clones were bred to C57BL/6 males to produce F_1 offspring and *CCN3*$^{+/-}$ mice were intercrossed to produce homozygous offspring (Supplementary Figure IVA, IVB). The deletion in the mRNA corresponding to the genomic deletion of the *CCN3* locus was confirmed using reverse-transcription polymerase chain reaction with cDNA generated from heart RNA that had been extracted from 28-day-old mice (Supplementary Figure IVC). *CCN3* protein was not detected in the aortas from *CCN3*$^{-/-}$ mice by immunohistochemistry (Figure 4B). Intercrosses between *CCN3*$^{+/-}$ animals produced viable offspring at the expected Mendelian frequency (data not shown). *CCN3*$^{-/-}$ animals developed normally to adulthood and both the males and females were fertile. The Table shows the background data for the 2-month-old *CCN3*$^{-/-}$ mice in comparison to their littermate controls. There were no obvious differences in body weight, systolic blood pressure, plasma glucose concentrations, and HbA_1c levels between the 2 groups. Hematoxylin and eosin staining and Masson trichrome staining of the aortas dissected from the 2-month-old mice showed that the vasculature appeared to have developed normally (Figure 5A). The amount of type III collagen, which is one of the main components of the extracellular matrix in the aorta,[19] also showed that there were no obvious changes in the amount of extracellular matrix because of the lack of *CCN3* (Figure 5A). Next, to evaluate the role of *CCN3* in the pathogenesis of neointimal hyperplasia, we injured the femoral arteries of the wild-type (n=6) and *CCN3*-null (n=6) male mice, using photochemically induced thrombosis. Histopathologic examination of the arteries 21 days after the injury revealed markedly enhanced neointimal thickening in the *CCN3*-null mice in comparison to the wild-type mice (Figure 5B). The mean intima-to-media ratios at 21 days after the injury were significantly higher in the arteries of the *CCN3*-null

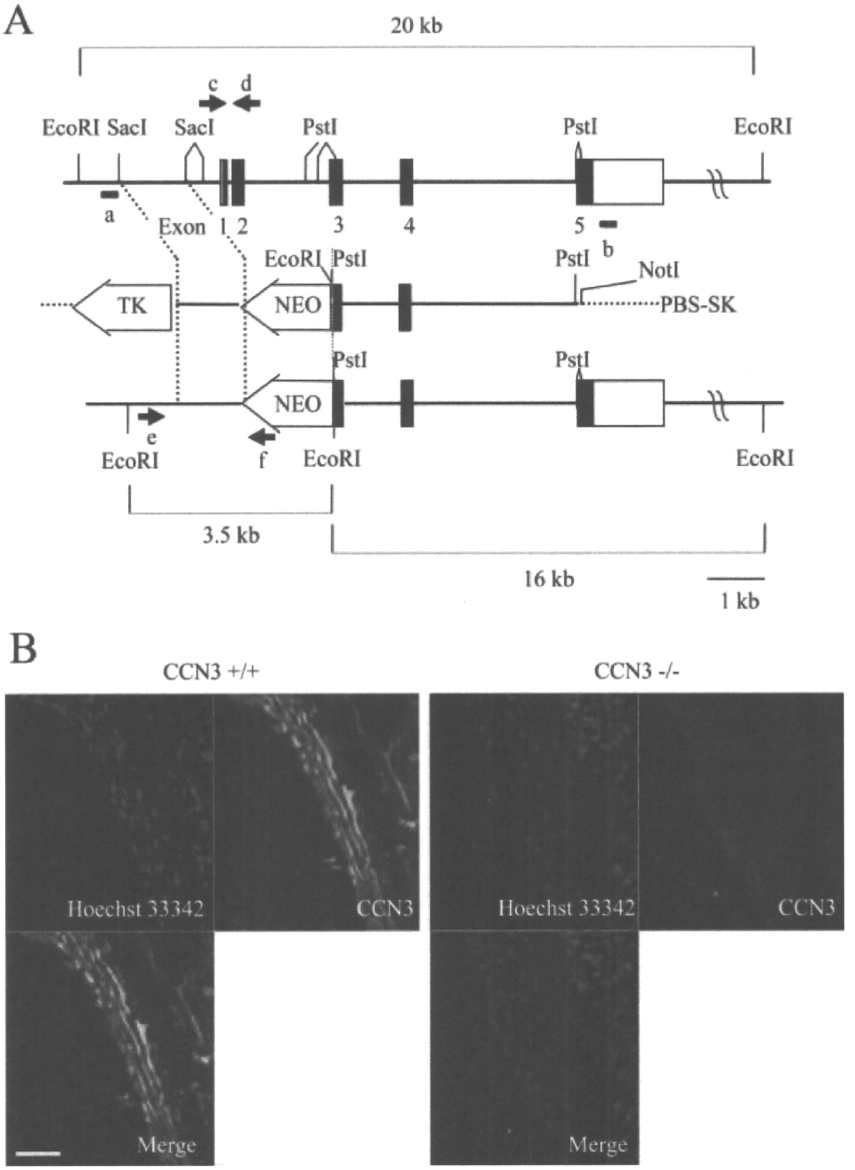

Figure 4. Generation of *CCN3*$^{-/-}$ mice. A, Genomic organization of the *CCN3* gene (top), targeting vector (middle), and targeted allele (bottom) were indicated. The targeting vector was constructed by replacement of the exon 1 to a part of 3 in *CCN3* genomic fragment with the PGK-neo cassette (*NEO*) and attachment of the HSV-tk cassette (*TK*) to its flank for the negative selection marker. B, Immunohistochemical staining of wild-type and mutant 2-month-old aorta with antibodies against *CCN3*. Bars=50 μm.

mice (1.193±0.071) than those of the wild-type mice (0.205±0.011; $P<0.01$; Figure 5C).

To understand how intimal thickening is enhanced in the *CCN3*-null mice, we studied cell proliferation and endothelialization after the vascular injury (Supplementary Figure VA, VB). We investigated the BrdU incorporated into the vascular wall 1 week after photochemically induced thrombosis. The number of BrdU-positive cells was higher in the aortas of the *CCN3*-null mice than in those of the control mice, indicating that the VSMC proliferated even in the absence of *CCN3*. We also investigated the endothelialization after antiplatelet endothelial cell adhesion molecule staining and found that, compared to the controls, endothelialization was reduced in the aortas of the *CCN3*-null mice.

We also examined platelet function by measuring the tail bleeding time (data not shown) and adventitial neovascularization by anti-PECAM-1 staining (Supplementary Figure VB). However, there were no differences in either the tail bleeding time or the adventitial neovascularization.

Table. Basic Characteristic of *CCN3*-Null Mice Compared to Littermate Controls

	Body weight, grams	Systolic blood pressure, mm Hg	Plasma glucose, mg/dL	HbA1c, %	N
CCN3$^{+/+}$	22.9±4.0	102.1±10.5	227.9±95.5	3.8±0.35	14
CCN3$^{-/-}$	23.2±3.6	113.6±19.4	198.1±104.0	3.5±0.38	17

CCN3 Expression Decreases in the Aorta of Streptozotocin-Induced Diabetic Mice

Finally, to determine the relevance of *CCN3* expression to disease conditions, we examined the *CCN3* expression in diabetic mice and found that it was significantly lower in the aorta of diabetic rats in comparison to control rats (Supplementary Figure VIA, VIB). Insulin treatment for reducing the

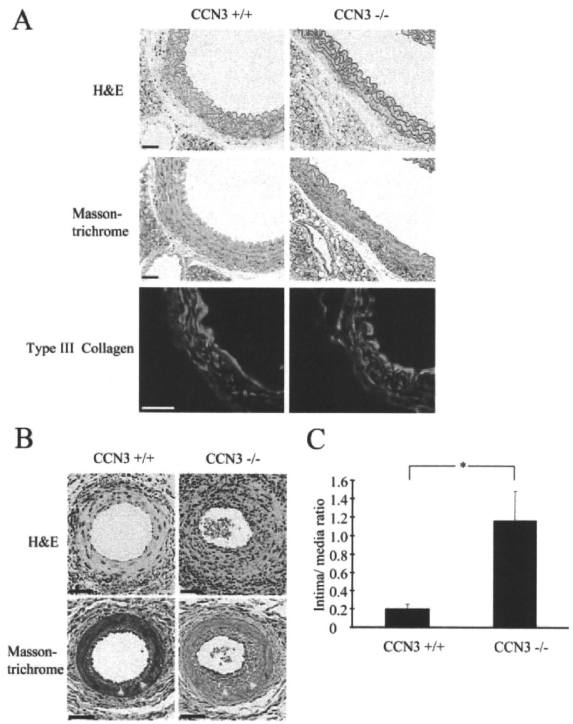

Figure 5. A histological examination of *CCN3*-null mice aorta and neointimal thickening in femoral arteries of wild-type and *CCN3*-null mice, which were induced by the photochemically induced thrombosis (Pit) method. A, Aortas were dissected from 2-month-old *CCN3*-null mice and wild-type controls and stained with hematoxylin and eosin, Masson trichrome, and anti-type III collagen antibody. B, Sections of femoral arteries, from wild-type controls and *CCN3*-null mice, at 21 days after endothelial injury were stained with hematoxylin and eosin and Masson trichrome, and representative cross-sections are shown. C, Intima-to-media (I/M) ratios at 21 days in wild-type and *CCN3*-null mice were calculated from cross-sectional areas morphometrically measured using an image analyzer. $^*P<0.01$ compared with wild-type controls. Bars=50 μm.

blood glucose level increased the *CCN3* expression in vessels, excluding the possibility that *CCN3* expression decreased because of the toxic effects of streptozotocin (Supplementary Figure VIC).

Discussion

This article reports 5 novel findings. First, the *CCN3* protein was expressed in the medial layer of the mouse aorta, especially in VSMC in vivo. Second, *CCN3* inhibited VSMC proliferation and migration. Third, *CCN3* inhibited VSMC proliferation independent of TGF-β signaling. Fourth, *CCN3* increased the expression of the cyclin-dependent kinase inhibitor, *p21*, at least partly through Notch signaling in VSMC. Fifth, *CCN3*$^{-/-}$ mice had a normal vascular phenotype under normal conditions; however, *CCN3* enhanced the neointimal hyperplasia in femoral arteries induced by endothelial injury.

Atherosclerosis is a leading cause of cardiovascular diseases around the world. VSMC migration and proliferation in the subendothelial space are pivotal steps in atherosclerosis development[20] and in restenosis formation after vascular intervention.[21] The recent development of drug-eluting stents, which release small amounts of antiproliferative agents locally, is an effective strategy for reducing restenosis,[22] which is primarily caused by the proliferation of VSMC. However, reducing the incidence of restenosis remains a considerable burden for the medical community. Therefore, the biological stimuli that inhibit VSMC proliferation and migration must be completely understood to address various clinical problems.

CCN3 plays potent roles in tumorigenesis,[2] chondrogenesis, skeletal and cardiac development,[23] and hematopoietic stem cell regulation.[24] However, the roles of *CCN3* in vessels are not yet fully understood. Ellis et al[8] precisely examined the expression of *CCN3* in the rat aorta and in the carotid artery. They localized *CCN3* mRNA expression to the smooth muscle cells in both the aorta and carotid artery. Further, they showed 7 days after injury to the carotid artery *CCN3* expression in the media is substantially reduced but that at the edge of the intima increases. At 14 days after the injury, the *CCN3* expression in the media remains low, but it is substantially increased throughout the intima in the VSMC. These observations strongly indicate that *CCN3* is involved in vascular ho-

meostasis, especially after vascular injury. Using immunohistology, we established that the *CCN3* protein is expressed in the smooth muscle cell layer in the mouse aorta. To our knowledge, this is the first in vivo report to confirm *CCN3* protein expression in aortic smooth muscle cells.

In agreement with the antiproliferative effects of *CCN3* in a large variety of cell types, we could also show that *CCN3* inhibited VSMC proliferation in vitro (Figure 2A, 2B). However, Ellis et al[8] reported that *CCN3* has no effect on VSMC proliferation. However, there were some significant differences in the experimental procedures used. The current study used human recombinant *CCN3*, which shares 80% amino acid identity with that of mouse *CCN3*. In contrast, Ellis et al used recombinant *CCN3* prepared using a baculovirus system. They also used a higher concentration of PDGF-BB and a different kind of fetal bovine serum, which induced higher proliferation rates than those seen in the current study. Therefore, the antiproliferative effects of *CCN3* may have been masked by the potent mitogenic stimulation. Furthermore, the antiproliferative effects of *CCN3* seemed transient (Supplementary Figure IB). Therefore, it might be difficult to determine these antiproliferative effects if the incubation time is longer than that used in this experiment.

The next series of experiments examined how *CCN3* inhibits VSMC proliferation. *CCN3* physically interacts with fibulin C,[25] integrins,[5] and connexin 43.[26] In addition, *CCN3* inhibits proliferation and differentiation through the Notch pathway.[17,27] Notch signaling dictates the cell fate and critically influences cell proliferation, differentiation, and apoptosis. It is observed in various tissues, including vessels. For instance, Notch ligands,[28] receptors,[29] and effectors[30] are expressed in VSMC in vivo. Furthermore, Notch signaling also plays a critical role in the correct architecture of vascular systems.[31] Therefore, we investigated the involvement of the Notch signaling pathway in the antiproliferative activity of *CCN3*. *CCN3* increased the expression of ICN1, whereas γ-secretase inhibitor reversed the antiproliferative effects of *CCN3* and partially inhibited the *CCN3*-induced upregulation of p21 (Figure 3C, 3D, and Supplementary Figure II); this indicated that the Notch signaling pathway was at least partially involved in the antiproliferative activity of *CCN3*. In addition, we examined the participation of TGF-β signaling in the *CCN3*-induced antiproliferative activity of VSMC, because TGF-β inhibits cell growth in a variety of cell types. Moreover, TGF-β and the Notch pathway cooperatively suppress epithelial cell growth.[32] However, anti-TGF-β neutralizing antibody could not reverse the *CCN3*-induced antiproliferative activity in VSMC (Figure 2B). Furthermore, *CCN3* had no effect on the phosphorylation of *Smad2*, which mediates TGF-β signaling and the activity of the plasminogen activator inhibitor-1 promoter, which contains the TGF-β–responsive element. *CCN3* also did not have any effect on the expression of the mRNA of either TGF-β or its receptors (data not shown). These results indicate that the inhibition of VSMC proliferation by *CCN3* is partially dependent on the Notch pathway but independent of TGF-β signaling.

Despite the growth inhibitory effects of *CCN3* in a wide variety of cell types, $CCN3^{-/-}$ mice were surprisingly viable and fertile. $CCN3^{-/-}$ mice could not be distinguished from their littermate controls by their gross appearance or vascular structure (Figure 5A).

CCN3 knockout mice were recently generated by another group.[23] Exon 3 of the *CCN3* gene was targeted ($NOV^{del3-/-}$) and some, but not all, of the $NOV^{del3-/-}$ mice were embryonically lethal and exhibited defects in both skeletal and cardiovascular development. However, $NOV^{del3-/-}$ mice produce a mutant form of the *CCN3* protein, which can be secreted and lacks only the von Willebrand factor (VWC) domain but contains 3 other intact functional domains. Furthermore, this phenotype is partly transmitted by dominant inheritance. Therefore, this protein is strongly suspected to result in the phenotypes observed in $NOV^{del3-/-}$ mice. In contrast, the mRNA in $CCN3^{-/-}$ mice lacked a region encoding 127 amino acids from the N-terminal end. This may result in a peptide that is translated from the fourth Methionine in complete *CCN3* mRNA and is not secreted because of the absence of the presequence required for secretion. Therefore, we believe that the presence of the mutant *CCN3* peptide only in $NOV^{del3-/-}$ leads to phenotypic differences between both types of mutant mice.

Although the vascular phenotype was normal under normal conditions, the enhancement of the intimal thickening in the *CCN3*-null mice after endothelial injury suggested that *CCN3* plays important roles in pathological situations and also indicated that *CCN3* inhibited VSMC proliferation and migration. Among the several methods that could induce the intimal thickening, such as flexible wire, balloon catheter, and laser injury, we chose the photochemically induced thrombosis method, which could induce intimal thickening constantly and relatively milder than the others.

It has also been reported that *CCN3* induces neovascularization. Further, we observed reduced endothelialization in *CCN3*-null mice. Therefore, increased VSMC proliferation and reduced endothelialization can affect the increased intimal thickening seen in the *CCN3*-null mice.

Finally, we studied *CCN3* expression in diabetic conditions and found that this expression was reduced in diabetic aortas as compared to the control aortas. Diabetic patients are prone to atherosclerotic vascular disease[33] and diabetic vascular lesions are prone to restenosis after angioplasty.[34] However, the mechanism by which atherogenesis is accelerated in patients with diabetes mellitus has not yet been determined. Because *CCN3* inhibited VSMC proliferation and migration, the reduced expression of *CCN3* might be linked with the accelerated atherogenesis in diabetes. So far, there have been few reports describing *CCN3* gene regulation. For instance, 1 report[35] describes that Wilms tumor 1, a transcriptional factor, binds to the *CCN3* promoter region and regulates its expression. In addition, the expression of the tumor suppressor gene *p53* depends on *CCN3* expression.[36] It therefore would be useful to investigate the precise transcriptional regulation of *CCN3* and seek pharmacological agents to prevent the

downregulation of *CCN3* in diabetic vessels to reduce the risk of diabetic vascular complications in the future.

In summary, this study demonstrated that *CCN3* is a regulator of VSMC proliferation and migration and of neointimal hyperplasia. Therefore, these results indicate the potential usefulness of this molecule in the modulation of atherosclerotic vascular disease.

Acknowledgments

The authors thank Reiko Kimura (Department of Clinical Cell Biology and Medicine, Chiba University Graduate School of Medicine) for her valuable technical assistance.

Sources of Funding

This study is supported by grants-in-aid for Scientific Research from the Ministry of Education, Culture, Sports, Science, and Technology; Ministry of Health, Labor, and Welfare; a grant from Mitsubishi Pharma Research Foundation; and a grant from the Takeda Scientific foundation.

Disclosures

None

References

1. Brigstock DR, Goldschmeding R, Katsube KI, Lam SC, Lau LF, Lyons K, Naus C, Perbal B, Riser B, Takigawa M, Yeger H. Proposal for a unified CCN nomenclature. *Mol Pathol.* 2003;56:127–128.
2. Perbal B. NOV story: the way to *CCN3*. *Cell Commun Signal.* 2006;4:3.
3. Perbal B. Pathogenic potential of myeloblastosis-associated viruses. *Infect Agents Dis.* 1995;4:212–227.
4. Gupta N, Wang H, McLeod TL, Naus CC, Kyurkchiev S, Advani S, Yu J, Perbal B, Weichselbaum RR. Inhibition of glioma cell growth and tumorigenic potential by *CCN3* (NOV). *Mol Pathol.* 2001;54:293–299.
5. Benini S, Perbal B, Zambelli D, Colombo MP, Manara MC, Serra M, Parenza M, Martinez V, Picci P, Scotlandi K. In Ewing's sarcoma *CCN3*(NOV) inhibits proliferation while promoting migration and invasion of the same cell type. *Oncogene.* 2005;24:4349–4361.
6. Jay P, Berge-Lefranc JL, Marsollier C, Mejean C, Taviaux S, Berta P. The human growth factor-inducible immediate early gene, CYR61, maps to chromosome 1p. *Oncogene.* 1997;14:1753–1757.
7. Ryseck RP, Macdonald-Bravo H, Mattei MG, Bravo R. Structure, mapping, and expression of fisp-12, a growth factor-inducible gene encoding a secreted cysteine-rich protein. *Cell Growth Differ.* 1991;2: 225–233.
8. Ellis PD, Chen Q, Barker PJ, Metcalfe JC, Kemp PR. Nov gene encodes adhesion factor for vascular smooth muscle cells and is dynamically regulated in response to vascular injury. *Arterioscler Thromb Vasc Biol.* 2000;20:1912–1919.
9. Matsumae H, Yoshida Y, Ono K, Togi K, Inoue K, Furukawa Y, Nakashima Y, Kojima Y, Nobuyoshi M, Kita T, Tanaka M. *CCN1* knockdown suppresses neointimal hyperplasia in a rat artery balloon injury model. *Arterioscler Thromb Vasc Biol.* 2008;28:1077–1083.
10. Cicha I, Yilmaz A, Klein M, Raithel D, Brigstock DR, Daniel WG, Goppelt-Struebe M, Garlichs CD. Connective tissue growth factor is overexpressed in complicated atherosclerotic plaques and induces mononuclear cell chemotaxis in vitro. *Arterioscler Thromb Vasc Biol.* 2005; 25:1008–1013.
11. Morisaki N, Takahashi K, Shiina R, Zenibayashi M, Otabe M, Yoshida S, Saito Y. Platelet-derived growth factor is a potent stimulator of expression of intercellular adhesion molecule-1 in human arterial smooth muscle cells. *Biochem Biophys Res Commun.* 1994;200:612–618.
12. Yokote K, Mori S, Hansen K, McGlade J, Pawson T, Heldin CH, Claesson-Welsh L. Direct interaction between Shc and the platelet-derived growth factor beta-receptor. *J Biol Chem.* 1994;269: 15337–15343.
13. Honjo S, Yokote K, Fujimoto M, Takemoto M, Kobayashi K, Maezawa Y, Shimoyama T, Satoh S, Koshizaka M, Takada A, Irisuna H, Saito Y. Clinical outcome and mechanism of soft tissue calcification in Werner syndrome. *Rejuvenation Res.* 2008;11:809–819.
14. Joyner AL. *Gene Targeting.* Oxford, UK: Oxford University Press; 1992.
15. Kikuchi S, Umemura K, Kondo K, Saniabadi AR, Nakashima M. Photochemically induced endothelial injury in the mouse as a screening model for inhibitors of vascular intimal thickening. *Arterioscler Thromb Vasc Biol.* 1998;18:1069–1078.
16. Roberts AB. Molecular and cell biology of TGF-beta. *Miner Electrolyte Metab.* 1998;24:111–119.
17. Katsuki Y, Sakamoto K, Minamizato T, Makino H, Umezawa A, Ikeda MA, Perbal B, Amagasa T, Yamaguchi A, Katsube K. Inhibitory effect of CT domain of *CCN3*/NOV on proliferation and differentiation of osteogenic mesenchymal stem cells, Kusa-A1. *Biochem Biophys Res Commun.* 2008;368:808–814.
18. Jin S, Hansson EM, Tikka S, Lanner F, Sahlgren C, Farnebo F, Baumann M, Kalimo H, Lendahl U. Notch signaling regulates platelet-derived growth factor receptor-beta expression in vascular smooth muscle cells. *Circ Res.* 2008;102:1483–1491.
19. Carrasco FH, Montes GS, Krisztan RM, Shigihara KM, Carneiro J, Junqueira LC. Comparative morphologic and histochemical studies on the collagen of vertebrate arteries. *Blood Vessels.* 1981;18:296–302.
20. Ross R. Atherosclerosis—an inflammatory disease. *N Engl J Med.* 1999; 340:115–126.
21. Ferns GA, Avades TY. The mechanisms of coronary restenosis: insights from experimental models. *Int J Exp Pathol.* 2000;81:63–88.
22. Stone GW, Moses JW, Ellis SG, Schofer J, Dawkins KD, Morice MC, Colombo A, Schampaert E, Grube E, Kirtane AJ, Cutlip DE, Fahy M, Pocock SJ, Mehran R, Leon MB. Safety and efficacy of sirolimus- and paclitaxel-eluting coronary stents. *N Engl J Med.* 2007;356:998–1008.
23. Heath E, Tahri D, Andermarcher E, Schofield P, Fleming S, Boulter CA. Abnormal skeletal and cardiac development, cardiomyopathy, muscle atrophy and cataracts in mice with a targeted disruption of the Nov (*CCN3*) gene. *BMC Dev Biol.* 2008;8:18.
24. Gupta R, Hong D, Iborra F, Sarno S, Enver T. NOV (*CCN3*) functions as a regulator of human hematopoietic stem or progenitor cells. *Science.* 2007;316:590–593.
25. Perbal B, Martinerie C, Sainson R, Werner M, He B, Roizman B. The C-terminal domain of the regulatory protein NOVH is sufficient to promote interaction with fibulin 1C: a clue for a role of NOVH in cell-adhesion signaling. *Proc Natl Acad Sci U S A.* 1999;96:869–874.
26. Fu CT, Bechberger JF, Ozog MA, Perbal B, Naus CC. *CCN3* (NOV) interacts with connexin43 in C6 glioma cells: possible mechanism of connexin-mediated growth suppression. *J Biol Chem.* 2004;279:36943–36950.
27. Sakamoto K, Yamaguchi S, Ando R, Miyawaki A, Kabasawa Y, Takagi M, Li CL, Perbal B, Katsube K. The nephroblastoma overexpressed gene (NOV/*CCN3*) protein associates with Notch1 extracellular domain and inhibits myoblast differentiation via Notch signaling pathway. *J Biol Chem.* 2002;277:29399–29405.
28. Villa N, Walker L, Lindsell CE, Gasson J, Iruela-Arispe ML, Weinmaster G. Vascular expression of Notch pathway receptors and ligands is restricted to arterial vessels. *Mech Dev.* 2001;108:161–164.
29. Leimeister C, Schumacher N, Steidl C, Gessler M. Analysis of HeyL expression in wild-type and Notch pathway mutant mouse embryos. *Mech Dev.* 2000;98:175–178.
30. Chin MT, Maemura K, Fukumoto S, Jain MK, Layne MD, Watanabe M, Hsieh CM, Lee ME. Cardiovascular basic helix loop helix factor 1, a novel transcriptional repressor expressed preferentially in the developing and adult cardiovascular system. *J Biol Chem.* 2000;275:6381–6387.
31. Roca C, Adams RH. Regulation of vascular morphogenesis by Notch signaling. *Genes Dev.* 2007;21:2511–2524.
32. Niimi H, Pardali K, Vanlandewijck M, Heldin CH, Moustakas A. Notch signaling is necessary for epithelial growth arrest by TGF-beta. *J Cell Biol.* 2007;176:695–707.
33. Andresen JL, Rasmussen LM, Ledet T. Diabetic macroangiopathy and atherosclerosis. *Diabetes.* 1996;45(Suppl 3):S91–S94.
34. Rozenman Y, Sapoznikov D, Mosseri M, Gilon D, Lotan C, Nassar H, Weiss AT, Hasin Y, Gotsman MS. Long-term angiographic follow-up of coronary balloon angioplasty in patients with diabetes mellitus: a clue to the explanation of the results of the BARI study. Balloon Angioplasty Revascularization Investigation. *J Am Coll Cardiol.* 1997;30:1420–1425.
35. Martinerie C, Chevalier G, Rauscher FJ III, Perbal B. Regulation of nov by WT1: a potential role for nov in nephrogenesis. *Oncogene.* 1996;12: 1479–1492.
36. Bohlig L, Metzger R, Rother K, Till H, Engeland K. The *CCN3* gene coding for an extracellular adhesion-related protein is transcriptionally activated by the p53 tumor suppressor. *Cell Cycle.* 2008;7:1254–1261.

On Line Supplement

Expanded Material and Methods

Reagents

Recombinant human CCN3, platelet-derived growth factor (PDGF)-BB and TGF-β were purchased from R&D Systems. Gamma secretase inhibitor was purchased from Calbiochem.

Cell Culture

Primary cultures of rat aortic SMC were isolated from 250-300 g Wister Rats. In brief, the tunica media was separated from the adventitia and endothelium by collagenase treatment. The cells were dispersed in collagenase and elastase and maintained in DMEM supplemented with 10% (vol/vol) FBS.

Semi-quantitative reverse transcription-PCR

Total RNA was isolated from cultured rat aortic VSMCs, as well as from several mouse tissues, using the RNeasy Mini Kit (Qiagen). One to 5 μg of total RNA was primed with Oligo dT primer and reversely transcribed using SuperScript III reverse transcriptase (Invitrogen). The polymerase chain reaction was performed in a 25 μl PCR reaction

containing 1 μl cDNA, Taq reaction buffer (Go Taq, Promega) and 10 μM dNTPs and the following primer sequence was used: p21 (Accession number: NM_080782) 5′-TCCACACAGGAGCAAAGTAT-3′and 5′-CGCTTGGAGTGATAGAAATC3′, p15 (NM_130812): 5′-GAGACGAGGCTGTAACAATC-3′ and 5′-CCTGCTCTTCAGCTAAGTCT-3′, CCN3 (NM_002514): 5′-CTATAAGCCAGGTTCTGTG-3′ and 5′-TTGCACTTGTAATGAACAGC-3′, TGF-β_1: (XM_001077389) 5′-TTTGAGGAGGGCAGCTTTTA-3′ and 5′-ACCAGTGAGGAGACCCAATG-3′, Hey1 (NP_034553) : 5′-GGGAAAGGGATGGTTGAGTT-3′ and 5′-ATGCTCAGATAACGGGCAAC-3′. GAPDH (NM_017008): 5′-GGCACAGTCAAGGCTGAGAAT-3′ and 5′-TCTCGCTCCTGGAAGATGGT-3′. The PCR was performed for 30-35 cycles, with each cycle consisting of 2 min denaturation at 94°C, 30 s of annealing at 55°C and 30 s of elongation at 72°C. The PCR amplification was followed by a 7 min final extension at 72°C. The size of the PCR amplification products were as follows: p21: 435 bp, p15: 413 bp, CCN3: 460 bp, TGF-β: 407 bp, Hey1: 567bp, GAPDH: 483 bp. GAPDH was used as an internal control. Ten μl of the PCR product were separated by electrophoresis on a 2% agarose gel (Ronza), which was then stained with an ethidium bromide solution (Sigma). The signals were photographed by a CCD camera system (Printograph,

ATTO) and densitometric analyses of fluorograms were performed using an image scanner (EPSON GT-X900) with the Scion image software program(Scion Corporation).

Proliferation Assay

For the BrdU incorporation, the VSMCs were plated at a density of 1 x 10^4 cells/well in a 96 well tissue culture plate. After 24 h serum starvation, the cells were treated with various concentrations of FBS or PDGF-BB in the presence of BrdU at 37°C in a humidified incubator containing 5% CO_2 for 24 hr. In the case of treatment with CCN3 and/or the neutralizing anti-TGF-β_1-β_2-β_3 antibody (R&D Systems), the cells were incubated with CCN3 and/or the anti-TGF-β antibody prior to adding the FBS or PDGF-BB. The incorporation of the BrdU into the DNA was detected using a monoclonal antibody against BrdU, followed by a fluorochrome-conjugated second antibody. The absorbance values were measured at 405 nm (reference 490 nm) using a microplate reader (SUNRISE remote, WAKO).

Migration Assay

The cell migration ability of SMC toward CCN3 was examined using a 96-well chemotaxis chamber. (AB96, Neuro Probe). A polyvinylpyrrolidone-free polycarbonate membrane with an 8.0 μm pore size (PFD8, Neuro Probe) was coated with 100 mg/ml of type I collagen (Vitrogen 100, Collagen Corp.) before use. For each set of experiments, any migration in the absence of CCN3 (considered to be random migration) served as the control and was referred to as 100% migration. Cell counts were made in a blinded manner. The experiments were performed in triplicate for every concentration of CCN3 and were repeated five times.

Western blotting

The cells were serum-starved for 24 hr and then incubated with 1 ng/ml TGF-β_1 or 100 ng/ml CCN3 for 30 min at 37°C. Next, the cells were lysed in boiling Laemmli's sample buffer and then subjected to SDS-10% polyacrylamide gel electrophoresis (PAGE). Immunoblotting was performed essentially as described before [1]. Briefly, the samples were blotted to nitrocellulose membrane (Hybond ECL, GE healthcare), the blots were blocked with 3% BSA and probed with the anti phospho-Smad 2 antibody (1:1000 dilution, Millipore), anti Smad 2/3 antibody (1:500 dilution, BD biosciences) overnight. Then the blots were washed and incubated either with peroxidase-conjugated anti rabbit

(1:2500 dilution, GE healthcare) or anti mouse (1:5000 dilution, Jackson Immunolaboratory) immunoglobulins. After washing, the sites of antibody binding were visualized using an ECL Western blotting detection system (GE healthcare).

Overexpression of RPMS-1 in VSMCs

cDNA plasmids containing RPMS-1 ORF were kindly provided by Professor Paul J Farrell (Imperial College Faculty of Medicine, London) [2]. Fifty thousand VSMCs were seeded in 12-well dishes. After 16 h of incubation, the cells were transfected with 0.6 μg of RPMS-1 construct by using Lipofectamine 2000 reagents (Invitrogen), according to the manufacturer's instructions. After transfection, the cells were serum-starved for 48 h. Next, the cells were incubated with or without CCN3 for 12 h. The gene expressions were analyzed using RT-PCR.

Effects of CCN3 on the cell cycle distribution of VSMCs

Effects of CCN3 on the cell cycle distribution of VSMCs

VSMCs were seeded with 60% confluence. After 16 h of incubation, the cells were starved for 24 h. The cells were then incubated with 100 ng/ml CCN3 or 1 ng/ml TGF-β in the presence or absence of FBS for 24 h. For cell-cycle analysis, the cells were

stained with 50 ug/ml propidium iodide (PI; Sigma Aldrich) as previously described [3], and the DNA content was analyzed by flow cytometry (FACSCalibur; BD Immunocytometry Systems, San Jose, CA)

Effects of CCN3 on PDGFR-ß expression and tyrosine phosphorylation and ERK activation

Sub-confluent VSMCs in 100-mm dishes were serum-starved for 24 h. The cells were then treated with 100 ng/ml CCN3 or 50 ng/ml PDGF-BB for 5 min at 37°C. After incubation, the cells were washed once with ice-cold PBS; solubilized with 1 ml of lysis buffer (50 mM TrisHCl [pH 7.4], 150 mM EDTA, 1% sodium deoxycholate, 1% Triton X100, and 0.1% SDS), 500 μM sodium orthovanadate, and complete protease inhibitor cocktail (Roche); placed on ice for 15 min; and centrifuged at 14,000*g* to remove insoluble materials. The supernatant (20 μl) was subjected to 10% SDS in order to examine the activation of ERK. To study PDGFR-ß expression and tyrosine phosphorylation, immunoprecipitation was performed as described earlier, using anti-PDGFR-ß antibody followed by absorption to protein G-Sepharose [4]. Immunoblotting was performed essentially as described above. The following commercial antibodies were used: mouse anti-p44/42 MAPK (1:1000 dilution, #9102) and mouse anti-phospho p44/42 MAPK (1:2000, #9106) (Cell Signaling).